# Validating the physical model of a chaotic system by topological analysis

Javier Used[1,*] and Juan Carlos Martín[2,†]
[1]*Nonlinear Dynamics, Chaos and Complex Systems Group, Departamento de Física Universidad Rey Juan Carlos, Tulipán s/n, 28933 Móstoles, Madrid, Spain*
[2]*Departamento de Física Aplicada, Universidad de Zaragoza, Pedro Cerbuna 12, 50009 Zaragoza, Spain*
(Received 25 February 2013; published 31 May 2013)

Topological analysis is employed for the first time to our knowledge as a method of validation for a physical model describing a chaotic system. Topological analysis theory provides both a way to characterize the topological structure of chaotic attractors by means of a set of integer numbers and a method to obtain this set departing from a time series generated by the chaotic system. The validation method proposed here consists of comparing the topological structure of chaotic attractors obtained from time series generated on the one hand by an experimental system and on the other hand by the numerical model under test. This procedure has been applied to an erbium-doped fiber laser subject to pump power sine-wave modulation.

DOI: 10.1103/PhysRevE.87.052921 PACS number(s): 05.45.Tp, 05.45.Ac, 42.65.Sf

## I. INTRODUCTION

Physics consists of modeling real systems. Reliable models provide many advantages in subsequent studies, as they make it possible to design and analyze new systems before their implementation. Usually, summarizing the properties of a system in a model is not trivial. This task becomes especially delicate when dealing with nonlinear systems. Little differences between two similar models generate very different responses even when they are working under the same conditions, and the same model with two similar parameters sets can give rise to very different responses. For these reasons model building has been a field of great interest for many years in the community of nonlinear dynamics [1]. Certainly a model cannot be accepted until validation, that is to say, after checking whether the real system and the model yield analog results. Again, model validation is a very complex task in nonlinear systems. Clearly there is an irreducible long-term error in the prediction of a system's state that is on the order of the chaotic attractor's size in phase space. Therefore, aspiring to a model capable of reproducing exactly the observed chaotic behavior is nonsense. Questions such as what should be compared and how the comparison should be carried out have led to the development of many tools for model validation in the last decades.

Modeling is a relatively broad concept, so it is important to state clearly what we mean here by this term. From a mathematical point of view, a model is a set of equations capable of reproducing the behavior of a system. Nevertheless, the terms model and modeling are employed in a physical context, in which the model is also capable of explaining the behavior of a system. From a physical point of view, model building starts from selecting the series of phenomena that have a non-negligible influence on the system's performance. As each phenomenon can be described by one or several equations, the interrelations between the different phenomena involved give rise to a set of equations. Obviously these equations contain parameters. They can present a certain experimental incertitude, but they are not free at all. If a good agreement is found between the results provided by the model and the experimental results (so that the model can be considered validated), physicists interpret that the system behavior has been understood: all the relevant phenomena have been correctly included in the model's equations. On the other hand, if the agreement is not good enough, either some relevant phenomenon has been ignored, or either the values of some parameters present in the model's equations had not been properly determined in previous measurements.

In order to compare a real chaotic system to its model, a possibility consists of comparing the statistical properties of the experimental and numerical attractors obtained. Quantities such as correlation dimension [2,3] or Lyapunov exponents [3–5] have been widely used. But it is well known that quite different attractors may have similar values of their statistical parameters [6], so obtaining an agreement between model and experiment for these parameters is only relatively meaningful [7]. Another procedure to validate a model consists of comparing the numerical and experimental bifurcation diagrams. It is admitted that bifurcation diagrams are a very useful form for presenting the dynamical evolution of a system [8]. Nevertheless, in many cases it is not viable to obtain such diagram for the experimental system. On the other hand comparisons between plots usually involve subjective criteria: certainly it is difficult to establish a quantitative formula to characterize how similar two bifurcation diagrams are. And, above all, similarity between bifurcation diagrams does not mean similarity between dynamical behaviors: these diagrams do not provide information about the attractors' structure. Other procedures have been proposed, based on other features of the attractor: location and stability of fixed points [9], Poincaré sections [10], geometry of attractors [11], and attractor symmetry [12].

In this work we propose topological analysis as a method for validating a model of a chaotic system. To date, application of topological analysis is restricted to systems whose phase space has three dimensions. Topological analysis techniques are based on the identification of unstable periodic orbits (UPOs) and on computation of the linking numbers between pairs of UPOs. The aim of the process is obtaining what is usually called a template. The template contains all the information about the attractor topology: the folding processes that cause

*javier.used@urjc.es
†jcmartin@unizar.es

 

each particular chaotic dynamics (together with stretching and squeezing) and the way all the UPOs are intertwined within the attractor. Topological analysis in general and templates in particular have been proven useful for identifying and describing different folding processes which generate chaos in numerical or experimental systems. For instance, topological analysis techniques together with the concept of a template have made possible identification of attractors embedded in a genus-1 torus whose mechanisms of generation were not the typical Smale horseshoe folding but other kinds of folding (reverse horseshoe [13–15], spiral [14–18], staple [15], or S [15]).

These ideas have been employed to compare if two attractors are topologically equivalent [19,20]. Due to this possibility, it has been claimed for many years that an important point of interest of topological analysis is its usefulness to test numerical models of experimental systems in a chaotic regime: a comparison of the templates obtained numerically and experimentally for different combinations of the control parameters would show clearly the model capabilities for prediction of the experimental system dynamics at quite a detailed level, concerning the very structure (or topology) of the chaotic attractors. Based on topological analysis, some mathematical models generated according to Ref. [21] have been validated [20,22,23]. Nevertheless, to our knowledge topological analysis has not been employed yet as a tool for validation of a physical model, that is to say, to compare data generated by any experimental system with the numerical solution generated by a physical model of this experimental system. The main aim of this work is to show how topological analysis can be useful for tests of this kind.

In addition, this work makes clear that the validity of an erbium-doped fiber laser (EDFL) model already tested for stable working conditions can be extended to working conditions in which the system response is chaotic. Success of the model relies on a characterization procedure previously developed by us [24], which leads to determination of the values to be introduced in the model's parameters. Therefore, validity of the model and of the characterization method are two tightly related questions.

The remainder of the paper is organized as follows. In Sec. II, an introduction to classical topological analysis is presented. A brief description of the EDFL model takes place in Sec. III. In Sec. IV we compare the results obtained applying the topological analysis to the time series corresponding to the model with those obtained from the experimental setup in a previous work. The main conclusions are provided in Sec. V.

## II. TOPOLOGICAL ANALYSIS

Applying topological analysis to physical systems was first proposed by Mindlin *et al*. [25] as a robust method to classify chaotic regimes.

A chaotic signal is generated when three mechanisms, stretching, folding, and squeezing act on flows in phase space [26]. The way that these mechanisms take place is a fingerprint of the dynamical system. On the one hand, topological analysis is a theory that provides the concepts and quantitative parameters suitable to characterize the attractors. On the other hand, it also provides a procedure to calculate the values of the different parameters from the time series generated by each particular dynamical system. These techniques were originally devised for dissipative systems whose phase space were three-dimensional, but they are also applicable to systems for which the flow rapidly relaxes to a three-dimensional subspace of its phase space. In all these cases, the Birman and Williams theorem [27,28] guarantees that there exists a two-dimensional object called a branched manifold (template and knot holder are also names used to refer to this object) such that it is possible to project a flow into this object while keeping their topological invariants unchanged. In particular, the UPOs present in the original attractor can be projected on the template in such a way that their linking and self-linking numbers remain unchanged. This template can be interpreted as a version of the attractor in the limit of infinite dissipation.

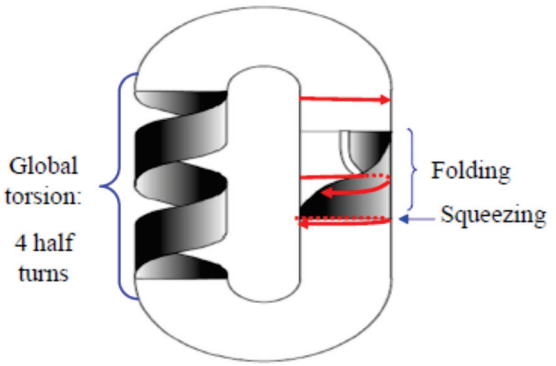


FIG. 1. (Color online) Typical scheme of a template.

The typical scheme of a template is shown in Fig. 1. It is a circuit-like strip with a twisted zone and another zone in which the section of the strip folds, giving rise to several branches. All the topological features of the attractor are summarized in the template, which is determined in a unique way by a set of integer numbers [25]. These integer numbers are related to the branches' torsions, the number of rotations of each branch around the others, and its piling order when the squeezing mechanism acts and all the branches converge in the original strip.

The procedure to determine the template ruling a given chaotic time series makes use of a fundamental property: there is a one-to-one relation between any orbit (periodic or not) and the sequence of template branches visited. If each branch is labeled (ordinarily by means of integers, the first one being 0), each periodic series of labels determines a unique UPO. In this way, the periodic sequence of labels is taken as the name of the UPO. A formula exists which allows one to calculate the linking number between two UPOs, given the sequence of branches visited by each orbit and the integer numbers that characterize the template [26,29,30].

A detailed revision of the procedure which leads to template determination can be found in [26]. Here we sum it up briefly. The first step is identification of some of the UPOs in the time series of the system. In order to do so, several techniques have been proposed [31–33]. Next, the linking numbers between each pair of UPOs are determined, as well as the self-linking number of each UPO with itself, which involves embedding the time series into a suitable three-dimensional phase space [26]. The process finishes with the search for a template compatible with all these linking numbers. When a generating partition

is previously known, the number of branches and the UPOs names can also be determined beforehand, which paves the way to template determination enormously. It suffices with a few linking numbers to determine the template unambiguously [30]. In the case that no previous generating partition is available, the way to proceed consists of starting with the simplest template, only with two branches, and try with all combinations of orbit names. If no combinations give rise to a valid solution, then we allow the template to have one more branch and the process starts again. The process is iterated until one or several solutions compatible with a combination of orbit names are found. In this case, frequently several templates are found to be compatible with the linking numbers calculated, and, in addition, the method does not guarantee that the minimum number of branches to get a compatible solution coincides with the authentic number of branches of the attractor.

Some additional ideas to this general treatment can be applied under certain conditions. If no tearing is observed in the Poincaré sections (PSs) (as in the case of EDFLs under study), the attractor can be embedded in a genus-1 torus. In this case, determinism and flow continuity impose tight relations between topological properties of the branches of the template (torsion of each branch, rotation around the other branches, and piling order). Due to this, the number of integer parameters necessary to characterize the template diminishes [30]: the torsion of the 0 branch ($T_{00}$) and the piling order suffice to characterize the template. Reduction in the number of characteristic parameters is important because it implies reduction in the number of linking numbers necessary to determine the template. This is especially important in experimental signals, in which often noise makes the counting of crossings between UPOs very troublesome. Therefore, in some cases just a few linking numbers can be determined with total certainty. On the other hand, for highly dissipative systems it is possible to obtain PSs equivalent to the branch line of the template. If a continuous PS parametrization is defined, the first-return map with regard to the parameter chosen is a thin line (the more dissipative the system, the thinner the line) with clear maxima and minima separating the different regions of the generating partition [14]. Application of this technique allows one to know the template number of branches and the symbolic name of each UPO before using the procedure described in the former paragraph. As explained there, it is very important to know beforehand the number of branches and the symbolic names in order to obtain a unique, reliable template.

## III. THE SYSTEM UNDER STUDY: THE ERBIUM-DOPED FIBER RING LASER

The scheme of a typical unidirectional EDFRL can be found in Ref. [34]. The model employed there is the one tested here, and it consists of the following nonautonomous system of two ordinary differential equations (so its phase space has three dimensions and topological analysis can be applied):

$$\frac{dN_{2r}(t)}{dt} = S_1(t) - S_2(t)N_{2r}(t) + S_3P_l(t) - S_4P_l(t)N_{2r}(t), \tag{1}$$

$$\frac{dP_l(t)}{dt} = P_l(t)[R_1 + R_2N_{2r}(t)], \tag{2}$$

where

$$S_1(t) = \frac{\gamma_a(\nu_p)}{h\nu_pN_T}P_p(t), \tag{3}$$

$$S_2(t) = \frac{[\gamma_a(\nu_p) + \gamma_e(\nu_p)]}{h\nu_pN_T}P_p(t) + \frac{1}{\tau}, \tag{4}$$

$$S_3 = \frac{\gamma_a(\nu_l)}{h\nu_lN_T}, \tag{5}$$

$$S_4 = \frac{[\gamma_a(\nu_l) + \gamma_e(\nu_l)]}{h\nu_lN_T}, \tag{6}$$

$$R_1 = \frac{c[\ln(T) - \gamma_a(\nu_l)L]}{D}, \tag{7}$$

$$R_2 = \frac{[\gamma_a(\nu_l) + \gamma_e(\nu_l)L]}{D}. \tag{8}$$

In the preceding coefficients, $h$ is the Planck constant, $N_T$ is the number of $Er^{3+}$ ions per unit length, $\tau$ is the laser transition lifetime, $\nu_p$ and $\nu_l$ are the pump and laser signal optical frequencies, $\gamma_a$ and $\gamma_e$ represent the absorption and emission coefficients, $T$ is the one trip transmission coefficient of the resonator ring, $L$ is the active medium length, $c$ is the speed of light in vacuum, and $D$ is the ring optical path. $P_p(t)$ is the pump power, in this case with a cosine wave profile: $P_p(t) = P_{p0}[1 + m\cos(\omega_e t)]$, where $P_{p0}$ stands for average pump power, $m$ is the modulation index, and $\omega_e$ is the excitation frequency.

In this system, the explicit state variables are $N_{2r}$ and $P_l$, which represent, respectively, the population of the upper laser transition level and the power of the laser signal averaged over the active medium. In the first equation, the first two contributions to $dN_{2r}(t)/dt$ account for pump absorption, pump stimulated emission, and spontaneous emission, while the last two terms account for laser signal absorption and laser signal stimulated emission. The second equation accounts for the phenomena that cause laser signal power variations: the losses due to the cavity passive elements (contained in $R_1$) and the amplification provided by the active medium.

Values of the different parameters contained in $S_i$ and $R_i$ have been experimentally determined. All of them are listed in Tables I and II. The parameters of Table I have been measured in a straightforward way by well-known methods, and those of Table II have been obtained from a characterization procedure detailed in Ref. [24]. In values in Table II, the experimental uncertainty is given explicitly for reasons that will be clear in next section.

TABLE I. Values of the model's parameters determined by means of straightforward measurements.

| | |
|---|---|
| Peak pump power wavelength | 1470 nm |
| Emission wavelength | 1532 nm |
| Cavity passive losses ($1 - T$) | 0.79 |
| Average launched pump power ($P_{p0}$) | 43 mW |
| Length of doped fiber ($L$) | 4.8 m |
| Total length of the ring | 37.5 m |
| Refraction index of the fiber core | 1.4674 |
| $^4I_{13/2}$ $Er^{3+}$ lifetime ($\tau$) | 10.1 ms |

TABLE II. Values of the model's parameters determined from the characterization procedure [24] and values employed in the numerical simulation.

| Parameter | Characterization | Simulation |
|---|---|---|
| $\gamma_a(\nu_p)$ | $0.66 \pm 0.07\ \mathrm{m}^{-1}$ | $0.651\ \mathrm{m}^{-1}$ |
| $\gamma_a(\nu_l)$ | $2.985 \pm 0.15\ \mathrm{m}^{-1}$ | $2.985\ \mathrm{m}^{-1}$ |
| $\gamma_a(\nu_p) + \gamma_e(\nu_p)$ | $0.80 \pm 0.07\ \mathrm{m}^{-1}$ | $0.825\ \mathrm{m}^{-1}$ |
| $\gamma_a(\nu_l) + \gamma_e(\nu_l)$ | $4.39 \pm 0.22\ \mathrm{m}^{-1}$ | $4.39\ \mathrm{m}^{-1}$ |
| $Er^{3+}$ lin. conc. ($N_T$) | $(3.64 \pm 0.35)\times 10^{13}$ ions/m | $3.64\times 10^{13}$ ions/m |

## IV. RESULTS

In a previous paper [15], we showed the templates obtained from the experimental time series emitted by the laser under study when its pump power is sine-wave modulated. For an average pump power of 43 mW and three different modulation depths ($m = 0.73$, $m = 0.78$, $m = 0.93$), we represented the different ranges of modulation frequencies where chaotic behavior was observed, and we pointed out the templates obtained in each range. In this way we obtained what we can call a template map. In order to analyze the validity of the model, we want to check whether the template map numerically generated for the same working conditions is similar to the experimental template map or not.

As a first step, before applying the topological analysis to the different numerical time series it is interesting to check whether the experimental and numerical distributions of chaotic regions coincide. In Figs. 2 (experimental results), 3, and 4 (numerical results), each vertical group of points represents the signal powers emitted at 20 time instants corresponding to 20 consecutive modulation periods at the same modulation phase. In some cases, the 20 points overlap, which shows that the output signal is periodic and the signal period is the same as the excitation one. In cases in which there are $n$ groups of overlapping points, there is a periodic response whose period is $n$ times the modulation one. If the 20 points are scattered, it is very likely that they belong to a chaotic time series. With these ideas in mind, it is very easy to appreciate in these figures the frequency ranges of periodic and (presumably) chaotic regimes.

Compare the numerical Figs. 3 and 4, and observe the values of the model's parameters employed to generate each figure given respectively in the columns "Characterization" and "Simulation" of Table II. Differences between the figures are quite significant despite the slight changes in the input parameters. Certainly, this is not a surprising fact in a

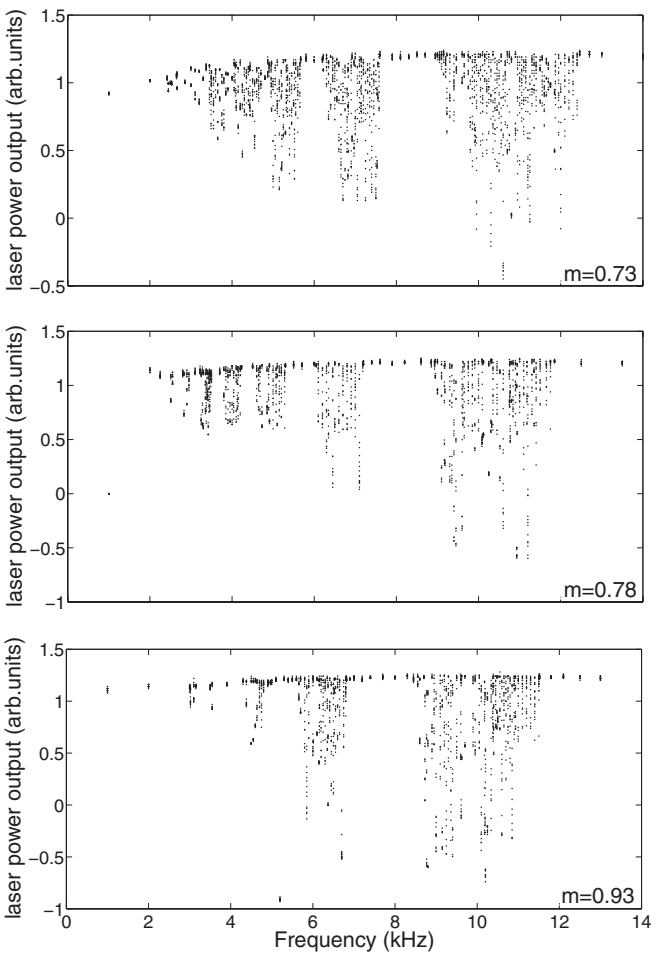


FIG. 2. Experimental bifurcation diagram.

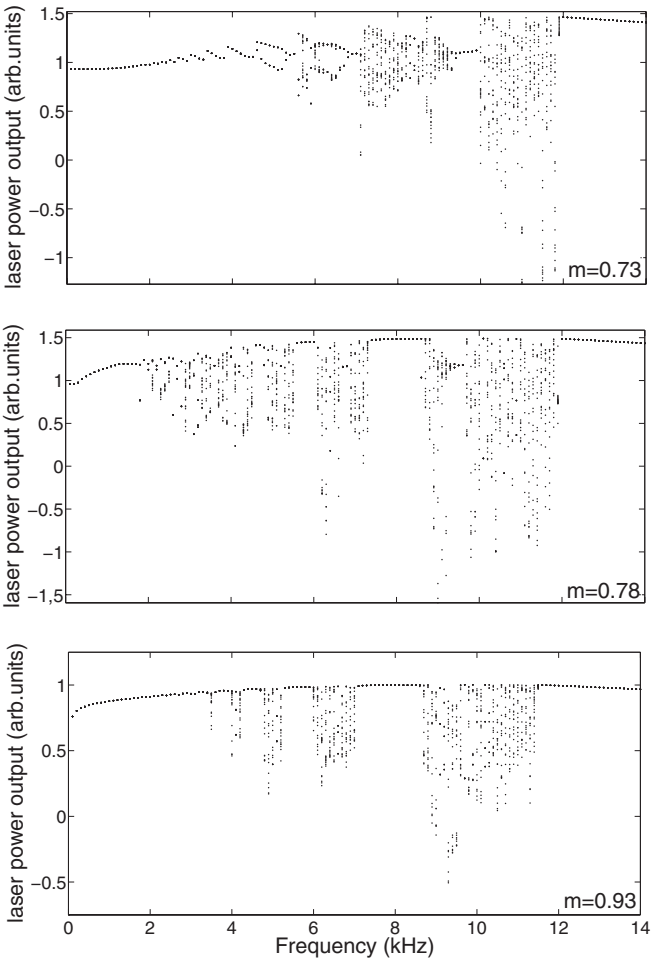


FIG. 3. Numerical bifurcation diagram calculated with the parameters of the column "Characterization" in Table II.

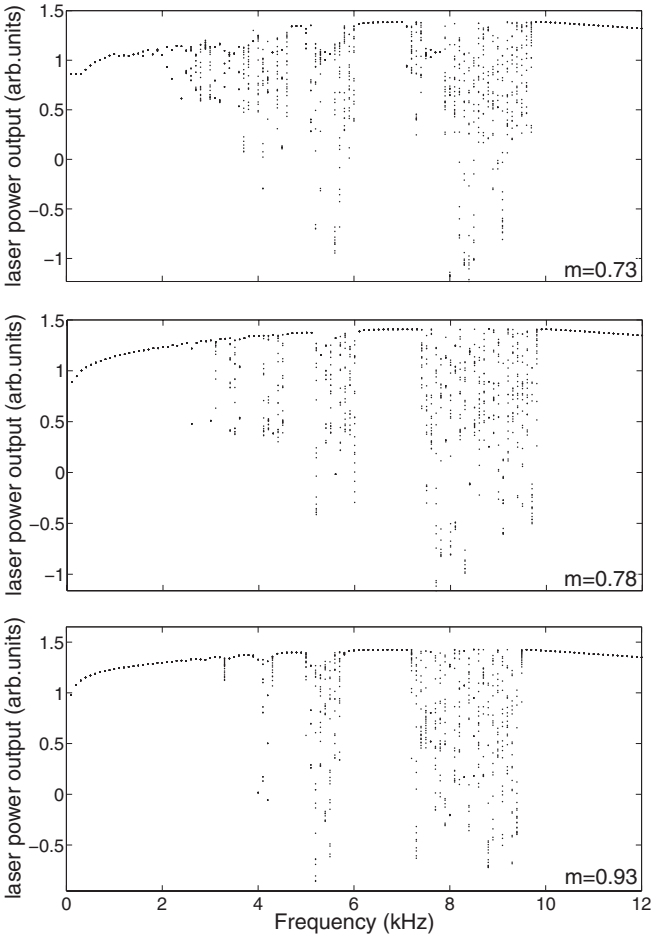


FIG. 4. Numerical bifurcation diagram calculated with the parameters of the column "Simulation" in Table II.

nonlinear system, but it illustrates the difficulties to find a good numerical-experimental agreement in nonlinear phenomena. Figures 3 and 4 are two representative figures out of many more obtained with different combinations of values in the model's parameters (not shown here for the sake of simplicity). In all cases, the values of the parameters were contained within its experimental uncertainty range. In particular, attending to the different frequency ranges of vertically scattered points, Fig. 4 is the one that shows the greatest similarity with the experimental Fig. 2, among the different figures calculated. For this reason, the values of the model's parameters employed to generate Fig. 4 are the ones we choose to carry out the calculations leading to the numerical template map.

For an average pump power of 43 mW and for the three modulation depth values mentioned before, different time

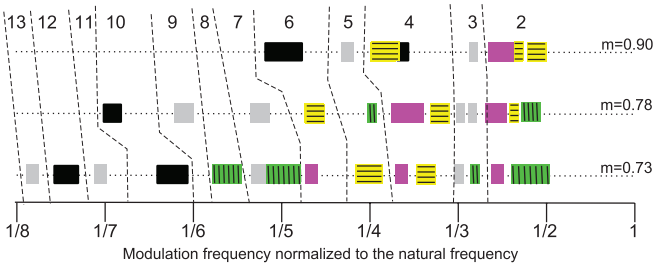


FIG. 6. (Color online) Summary of the theoretical templates found as a function of the pump modulation frequency and modulation index. Theoretical templates have been obtained from time series generated by the model [Eqs. (1) and (2)], employing the parameters of Table I and Table II (column "Simulation"). Colors and patterns show the "species" of template according to Fig. 5. Labels at the top of each sector show $T_{00}$, which is the torsion of the corresponding red branch in Fig. 5, expressed in number of half turns.

series have been calculated by sweeping the modulation frequency over the 1 kHz–21 kHz band; at 50 Hz steps, 21 kHz is the natural laser frequency for CW pump power of 43 mW. Hereafter we will refer to it as $f_r$. Each series contains around $10^4$ modulation periods, which is sufficient to apply topological analysis techniques in a reliable way. Results are summarized in Fig. 6, to be compared to the experimental template map obtained in Ref. [15] (Fig. 7). The color code employed in both figures is established in Fig. 5.

In order to value the capabilities of the model employed here, compare Figs. 6 and 7. Obviously, Fig. 6 is quite far from fitting to Fig. 7 perfectly, but take several circumstances into account. First, it deals with the model of a nonlinear system. It is inherent to the nature of a nonlinear system to behave in a way strongly dependent on small variations in the values of the model's parameters (smaller than the experimental incertitude, as shown by Figs. 3 and 4). And, second, consider also that the model does not have any free fitting parameter. Due to these circumstances, expecting a close coincidence between experimental and model results would be unrealistic. In order to compare the experimental response with the model forecast, we believe that the interesting aspects concern the global structure of both figures. Comparison of Figs. 6 and 7 makes clear that the model is capable of predicting the approximate location of the chaotic regions as well as the structure of the template map: as it was obtained in the experiment, the numerical calculations also yield template regions of global torsion $\theta$ (integer part of $T_{00}/2$) located approximately around $f = f_r/\theta$. It must be recognized that in Fig. 6 these regions appear shifted towards the left with regard to Fig. 7, which could be due to the experimental parameters,

| Species | Horseshoe | Reverse horseshoe | Out-to-in spiral | In-to-out spiral | Staple | S | Reverse out-to-in spiral | Reverse in-to-out spiral | Reverse staple | Out-to-in spiral |
|---|---|---|---|---|---|---|---|---|---|---|
| Code Figs. 5-6 | | | | Not found | | | | Not found | | |
| Insertion matrix | (0 1) | (1 0) | (0 2 1) | (1 2 0) | (0 2 1) or (1 2 0) | (2 1 0) | (2 0 1) | (1 0 2) | (1 0 2) or (2 0 1) | (0 3 1 2) |
| Sketch of the folding process | | | | | | | | | | |

FIG. 5. (Color online) Folding processes characteristic of the different species of templates treated in this work.

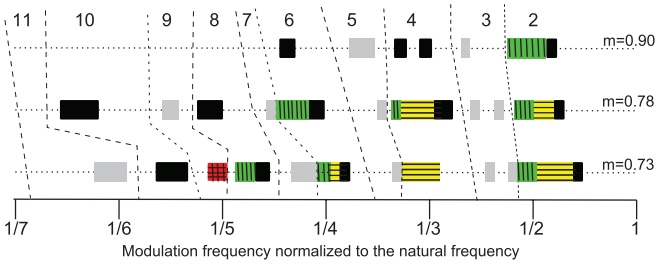


FIG. 7. (Color online) Summary of the experimental templates found as a function of the pump modulation frequency and modulation index. Colors and patterns show the species of template according to Fig. 5. Labels at the top of each sector show $T_{00}$, which is the torsion of the corresponding red branch in Fig. 5, expressed in number of half turns.

whose precise determination is a really complex matter. But, in general, it can be said that the model explains satisfactorily the system behavior in chaotic regime from a general point of view. From a more detailed perspective, we find some striking similarities and also some differences. Figure 8 (top) compares an experimental PS with a numerical one, both obtained by stroboscopic sampling and corresponding to the same chaotic region [$m = 0.73$, $T_{00} = 4$, and $I = (0\ 2\ 1)$]. Coincidence is very high between the experimental one and the part of the numerical one enclosed in the square. Although quite apparent, the region outside the square is not really significant: it corresponds to small values represented in logarithmic scale, impossible to obtain in the experimental case due to the detector noise. In Fig. 8 (bottom), one can note the excellent coincidence between the experimental and numerical profiles of the UPOs $\overline{1}$ and $\overline{10}$ extracted from the corresponding time series.

Concerning the differences, two are the most remarkable: on the one hand, in the numerical results, the $S$ structure [behavior marked in Fig. 7 with a dark (red) rectangle with a squared pattern] has not been observed; on the other hand, templates of four branches have been obtained in calculations but were not identified in the experimental data. The experimental $S$ structure has been observed for a very specific range of control parameters, so it could be expected that maybe it would appear if we introduced other combination of parameters values. We have tried with different combinations without success. Therefore, we have not been able to prove that the model can generate a time series ruled by an $S$ template, but certainly neither does its absence in our numerical results prove the opposite. With regard to templates with four branches, let us analyze the example of Fig. 9 together with Table III. The first return map, obtained according to the procedure established in Ref. [14], shows two maxima and a minimum. In this way we identify four branches, and we can guess the symbolic name of almost all the UPOs pointed out in Fig. 9. The exceptions are orbits **5b** and **6a**, because some of their points in the first return map are located in some of

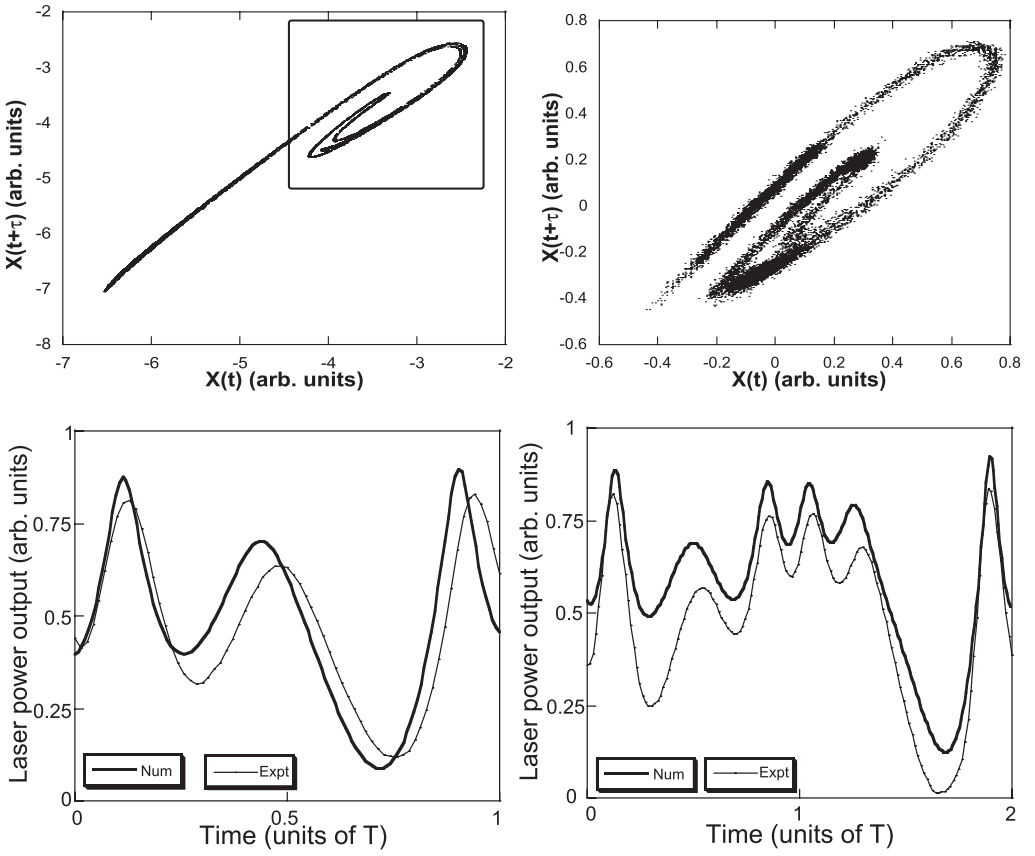


FIG. 8. Top: Comparison of a numerical (left) and an experimental (right) Poincaré section. Bottom: Comparison of the UPOs $\overline{1}$ (left) and $\overline{10}$ (right) obtained experimental and numerically. In the horizontal axis, T represents the period of the pump power modulation.

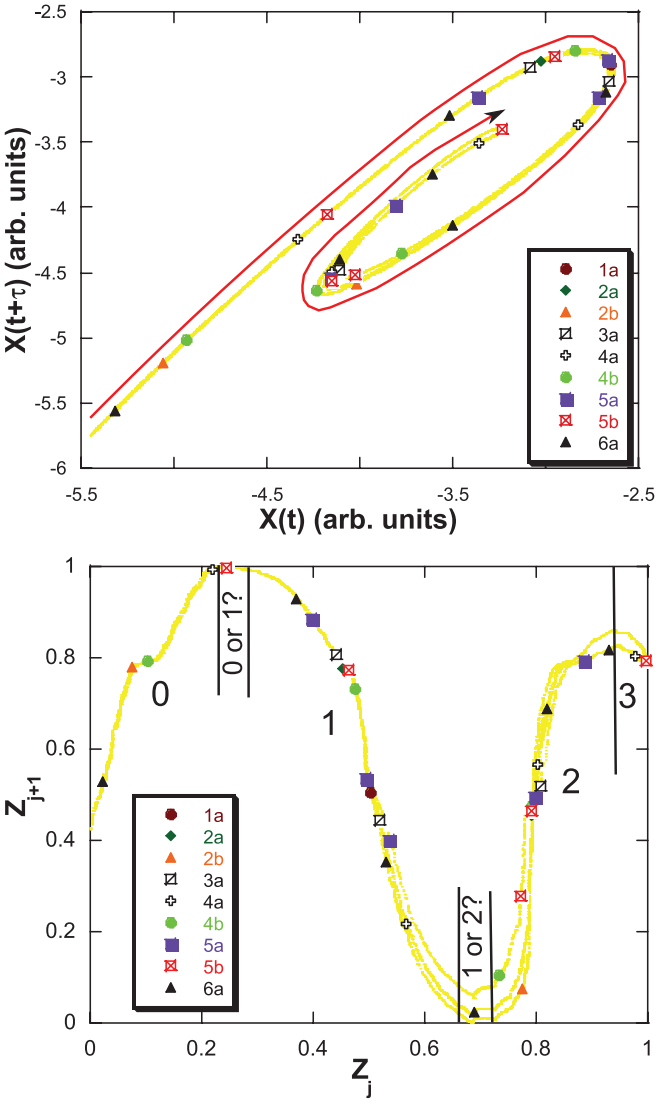


FIG. 9. (Color online) Top: Poincaré secction corresponding to the the four branches template obtained by stroboscopic sampling. The different dots represent intersections of different UPOs with the Poincaré section. Bottom: First return map as a function of the $Z$ parameter [14] obtained from the Poincaré section of the upper figure. (According to Ref. [14], $Z$ is defined as the coordinate along the arrow appearing in the figure, normalized so that $Z = 0$ for the arrow tail and $Z = 1$ for the arrow head. For any point of the $PS$, its $Z$ coordinate is defined as the $Z$ coordinate of its closest point which belongs to the arrow). The different dots represent the $Z$ parameters corresponding to UPO intersections. The lines demarcate the approximate borders between the regions in the generating partition [15]. The UPOs names appearing in the legend contain a number expressing the corresponding UPO period.

the incertitude regions between branches. Concretely, orbit **5b** might be $\overline{12032}$ or $\overline{12132}$, while orbit **6a** might be $\overline{112210}$ or $\overline{112220}$. The only template with four branches compatible with all the linking numbers and all the orbit names (Table III) is an outside-to-inside spiral template with $T_{00} = 6$.

Observe that in this case the information provided by the first return map is key for correct template determination: without the first return map, we would not know beforehand

TABLE III. Linking numbers between the different UPOs obtained from the temporal signal corresponding to Fig. 9.

| | $\overline{1}$ | $\overline{12}$ | $\overline{20}$ | $\overline{112}$ | $\overline{1032}$ | $\overline{1202}$ | $\overline{11122}$ | **5b** | **6a** |
|---|---|---|---|---|---|---|---|---|---|
| $\overline{1}$ | 0 | | | | | | | | |
| $\overline{12}$ | 7 | 7 | | | | | | | |
| $\overline{20}$ | 7 | 14 | 7 | | | | | | |
| $\overline{112}$ | 11 | 22 | 21 | 22 | | | | | |
| $\overline{1032}$ | 15 | 30 | 28 | 45 | 45 | | | | |
| $\overline{1202}$ | 14 | 29 | 28 | 43 | 58 | 43 | | | |
| $\overline{11122}$ | 18 | 37 | 35 | 55 | 75 | 72 | 74 | | |
| **5b** | 18 | 37 | 35 | 55 | 75 | 73 | 93 | 74 | |
| **6a** | 22 | 44 | 42 | 66 | 88 | 86 | 110 | 110 | 107 |

either how many branches we have or the UPOs' symbolic names. As explained before, sometimes template determination is possible even without knowledge of these data, by means of the topological analysis program systematized in Ref. [26], but in this case application of this program without the information of the orbits' symbolic names yields that a spiral with three branches and $T_{00} = 6$ is compatible with the linking numbers obtained. Therefore, by means of this procedure the existence of a fourth branch would not be revealed. Considering the reasons why a template with four branches like this has not been experimentally observed, we find that the fourth branch (labeled "branch 3" in Fig. 9) is short enough to become masked by noise in an experimental first return map. For a clear experimental observation of a template with four branches, it would be necessary that the fourth branch was longer in order to appreciate it in a first return map and/or gave rise to UPOs whose linking numbers were not compatible with any template with three branches.

## V. CONCLUSIONS

Topological analysis has been proved useful as a method for testing the validity of a physical model candidate to describe the behavior of an experimental chaotic system. In the case of an EDFL, studied here, topological analysis shows how the model is not only capable of explaining the distribution of periodic and chaotic regions in the space of the control parameters, but also the topological structure of the chaotic attractors found in each region. This fact proves that the EDFL model employed accounts for all the relevant phenomena necessary to explain not only the appearance of chaotic behavior but also much subtler details concerning the structure of the attractors found.

This work shows that, despite some weaknesses of topological analysis, it is a method that deserves to be considered for model validation. In our opinion, its main weakness is its limited domain of application to systems whose phase space has three dimensions, and that is why currently there are researchers trying to extend topological analysis to higher dimensions. On the other hand, it requires working with relatively large time series, which entails suitable experimental equipment and a subsequent careful analysis. The bottleneck is experimental acquisition of a suitable time series, but this operation is perfectly feasible nowadays, save for phenomena

with very fast characteristic times or for very unstable systems. Concerning the amount of work necessary to process all the time series, it must be recognized that it is considerable, but in exchange topological analysis offers the advantage of dealing with concepts such as the structure of attractors and the folding processes that generate them. These concepts are much more suitable than any statistical parameter to compare attractors and, therefore, to validate physical models. We think that the amount of work required by topological analysis is by far compensated by the fistrength of the results that it provides.

## ACKNOWLEDGMENT

This work was supported by the Spanish Ministry of Science and Innovation under Projects No. FIS2009-09898 and FIS2010-20821.

[1] J. P. Crutchfield and B. S. McNamara, Complex Syst. **1**, 417 (1987).
[2] R. Bakker, J. C. Schouten, C. L. Giles, F. Takens, and C. M. van den Bleek, Neural Comput. **12**, 2355 (2000).
[3] M. Small and C. K. Tse, Phys. Rev. E **66**, 066701 (2002).
[4] K. H. Chon, J. K. Kanters, R. J. Cohen, and N. H. Holstein-Rathlou, Physica D **99**, 471 (1997).
[5] E. M. A. M. Mendes and S. A. Billings, Int. J. Bifurcation Chaos Appl. Sci. Eng. **7**, 2593 (1997).
[6] C. Letellier, T. D. Tsankov, G. Byrne, and R. Gilmore, Phys. Rev. E **72**, 026212 (2005).
[7] T. P. Lim and Puthusserypandy, Chaos **16**, 0131106 (2006).
[8] Y. V. Kolokolov and A. V. Monovskaya, Int. J. Bifurcation Chaos Appl. Sci. Eng. **16**, 85 (2006).
[9] D. Allingham, M. West, and A. I. Mees, Int. J. Bifurcation Chaos Appl. Sci. Eng. **8**, 2191 (1998).
[10] B. P. Bezruchko, A. S. Karavaev, V. I. Ponomarenko, and M. D. Prokhorov, Phys. Rev. E **64**, 056216 (2001).
[11] G. Boudjema and B. Cazelles, Chaos Solitons Fractals **12**, 2051 (2001).
[12] L. A. Aguirre, R. A. M. Lopes, G. F. V. Amaral, and C. Letellier, Phys. Rev. E **69**, 026701 (2004).
[13] G. Boulant, S. Bielawski, D. Derozier, and M. Lefranc, Phys. Rev. E **55**, R3801 (1997).
[14] J. Used, and J. C. Martín, Phys. Rev. E **79**, 046213 (2009).
[15] J. Used and J. C. Martín, Phys. Rev. E **82**, 016218 (2010).
[16] G. Boulant, M. Lefranc, S. Bielawski, and D. Derozier, Int. J. Bifurcat. Chaos **8**, 965 (1998).
[17] L. Kocarev, Z. Tasev, and D. Dimovski, Phys. Lett. A **190**, 399 (1994).
[18] C. Letellier, G. Gouesbet, and N. F. Rulkov, Int. J. Bifurcat. Chaos **6**, 2531 (1996).
[19] C. Letellier and G. Gouesbet, J. Phys. II **6**, 1615 (1996).
[20] N. B. Tufillaro, P. Wyckoff, R. Brown, T. Schreiber, and T. Molteno, Phys. Rev. E **51**, 164 (1995).
[21] R. Brown, N. F. Rulkov, and E. R. Tracy, Phys. Rev. E **49**, 3784 (1994).
[22] C. Letellier, L. Le Sceller, E. Maréchal, P. Dutertre, B. Maheu, G. Gouesbert, Z. Fei, and J. L. Hudson, Phys. Rev. E **51**, 4262 (1995).
[23] L. A. Aguirre, and C. Letellier, Math. Probl. Eng. **2009**, 238960 (2009).
[24] I. J. Sola, J. C. Martín, and J. M. Álvarez, Opt. Commun. **203**, 349 (2002).
[25] G. B. Mindlin, X.-J. Hou, H. G. Solari, R. Gilmore, and N. B. Tufillaro, Phys. Rev. Lett. **64**, 2350 (1990).
[26] R. Gilmore and M. Lefranc, *The Topology of Chaos* (Wiley, New York, 2011).
[27] J. S. Birman and R. f. Williams, Topology **22**, 47 (1983).
[28] J. S. Birman and R. F. Williams, Contemp. Math. **20**, 1 (1983).
[29] L. LeSceller, C. Letellier, and G. Bouesber, Phys. Rev. E **49**, 4693 (1994).
[30] J. C. Martín and J. Used, Int. J. Bifurcation Chaos Appl. Sci. Eng. **19**, 3803 (2009).
[31] F. Papoff, A. Fioretti, E. Arimondo, G. B. Mindlin, H. Solari, and R. Gilmore, Phys. Rev. Lett. **68**, 1128 (1992).
[32] M. Lefranc, P. Glorieux, F. Papoff, F. Molesti, and E. Arimondo, Phys. Rev. Lett. **73**, 1364 (1994).
[33] P. So, E. Ott, T. Sauer, B. J. Gluckman, C. Grebogi, and S. J. Schiff, Phys. Rev. E **55**, 5398 (1997).
[34] I. J. Sola, J. C. Martín, and J. M. Álvarez, Opt. Commun. **212**, 359 (2002).